JACS Au
AN OPEN ACCESS JOURNAL OF THE AMERICAN CHEMICAL SOCIETY

pubs.acs.org/jacsau

Article

A New Pathway for CO_2 Reduction Relying on the Self-Activation Mechanism of Boron-Doped Diamond Cathode

Jinglun Du, Andrea Fiorani, Taichi Inagaki, Atsushi Otake, Michio Murata, Miho Hatanaka, and Yasuaki Einaga*

Cite This: *JACS Au* 2022, 2, 1375−1382

Read Online

ACCESS | Metrics & More | Article Recommendations | Supporting Information

ABSTRACT: By means of an initial electrochemical carbon dioxide reduction reaction (eCO_2RR), both the reaction current and Faradaic efficiency of the eCO_2RR on boron-doped diamond (BDD) electrodes were significantly improved. Here, this effect is referred to as the self-activation of BDD. Generally, the generation of carbon dioxide radical anions ($CO_2^{\bullet-}$) is the most recognized pathway leading to the formation of hydrocarbons and oxygenated products. However, the self-activation process enabled the eCO_2RR to take place at a low potential, that is, a low energy, where $CO_2^{\bullet-}$ is hardly produced. In this work, we found that unidentate carbonate and carboxylic groups were identified as intermediates during self-activation. Increasing the amount of these intermediates via the self-activation process enhances the performance of eCO_2RR. We further evaluated this effect in long-term experiments using a CO_2 electrolyzer for formic acid production and found that the electrical-to-chemical energy conversion efficiency reached 50.2% after the BDD self-activation process.

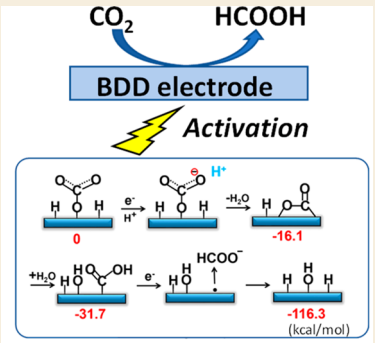

Enhanced electrochemical CO_2 reduction

KEYWORDS: *boron-doped diamond, CO_2 reduction, self-activation, energy conversion efficiency, intermediates*

1. INTRODUCTION

Research on carbon dioxide (CO_2) utilization is one of the keystones to realize the artificial carbon cycle and possibly carbon neutrality.[1,2] Several methods are currently under investigation,[3,4] and among them, the electrochemical CO_2 reduction reaction (eCO_2RR) has been proved to be a viable and efficient approach to reduce CO_2 into small useful molecule compounds like CO,[5] formic acid, or short chain hydrocarbons and oxygenates.[6−8] In these products, as a liquid fuel, formic acid not only possesses superiorities in transportation and storage but also has a bright application prospect in hydrogen vector[9] and fuel cells.[10] However, high overpotentials, poor product selectivity, and low current densities are still obstacles that hinder the technological applications of eCO_2RR.[11]

During eCO_2RR, the main reason concerning overpotentials and poor product selectivity was found to be the energetically unfavorable CO_2 adsorption.[12] Specific interactions between the CO_2 molecule (i.e., substrate) and electrodes (i.e., electrocatalyst) are needed to stabilize reaction intermediates, leading to lower overpotentials, high product selectivity, and faster reaction rate. Until now, the most recognized pathway for eCO_2RR is through the generation of CO_2 radical anion ($CO_2^{\bullet-}$).[13] If the generation of $CO_2^{\bullet-}$ is the rate-determining step, then this will introduce a large overpotential, as $CO_2/CO_2^{\bullet-}$ redox couple has a standard potential that lies near −1.85 V vs SHE which limits the electrolysis potential in a highly negative range.[13−17]

Kanan's group reported that compared to pure metal, oxidized or oxide-derived metal electrodes showed more prominent Faradaic efficiency and reduced overpotential for eCO_2RR,[18,19] where the increased stabilization of $CO_2^{\bullet-}$ intermediate was speculated to be the reason for this improved performance. But unfortunately, the chemical model and direct evidence of the interaction between CO_2 molecules and the oxygen-terminations are still unclear. In this context, the surface state of the electrode is crucial to provide stabilization for intermediate species in reaction mechanisms which did not rely on the generation of $CO_2^{\bullet-}$. A possible pathway has been proposed by Baruch et al. as the mechanism involved bicarbonate functional groups and an unlikely simultaneous transfer of two electrons.[20] Valenti et al. proposed CeO_2 as an electrocatalyst for CO_2 hydrogenation at overpotential as low as −0.02 V.[21] From the previous examples, it is clear that oxides or oxygenated species play a central role in eCO_2RR at low overpotentials. Therefore, the specific mechanism for eCO_2RR, especially when the applied potential is insufficient to form $CO_2^{\bullet-}$ radicals, is still worth further investigation.

Received: February 9, 2022
Revised: April 26, 2022
Accepted: May 9, 2022
Published: May 23, 2022

https://doi.org/10.1021/jacsau.2c00081
JACS Au 2022, 2, 1375−1382

Boron-doped diamond (BDD) was proposed as an outstanding candidate for mechanistic investigation of eCO_2RR. BDD is chosen for its long-term stability,[22] resistance to corrosion,[23] and high product selectivity[24,25] in eCO_2RR. In addition, due to its unique properties of low capacitive current and wide potential window,[26] BDD not only could greatly inhibit the reactivity of hydrogen evolution, which is the main competitor of eCO_2RR, but also is able to show evident redox signals for the electrochemical analysis. However, so far, the mechanism for the initial eCO_2RR reaction process has not been clearly determined. Therefore, in order to apply eCO_2RR to industrial processes, we now urgently need clarification and optimization of the factors that determine the experimental conditions, including the pretreatment of BDD electrode surfaces.

Here, we investigated a process referred as "self-activation" of BDD that prompted us to suggest a new and efficient pathway for eCO_2RR, which bypasses the mechanism involving $CO_2^{\bullet-}$. During electrolysis, the CO_2 molecules were first bound by BDD in the form of unidentate carbonate ($-O-CO_2$) and were further transformed to carboxylic structure ($-COOH$) after a proton and electron transfer reaction. This process leaves a detectable amount of carboxylic groups on the surface of BDD which are dependent on time, current density, and potential, for this reason named self-activation, finally enhancing the performance in terms of Faradaic efficiency and partial current density. The application of this self-activation mechanism was evaluated on the performance of eCO_2RR with a long-term two-electrode electrolysis reaching a remarkable electrical-to-chemical energy (ECE) conversion efficiency of 50.2% after 7 h of self-activation at the total cell voltage of 2.7 V for eCO_2RR to formic acid.

2. EXPERIMENTAL SECTION

2.1. Materials

KCl, KOH, H_2SO_4, $NaClO_4$, and 2-propanol were purchased from Wako Pure Chemical Industries Ltd. $NiSO_4$, $FeSO_4$, and $(NH_4)_2SO_4$ were purchased from Sigma-Aldrich. All reagents were used without any further purification. The deionized (DI) water employed in this work was from a Simply-Lab water system (DIRECT-Q 3 UV, Millipore) with a resistivity of 18.2 MΩ·cm at 25 °C. Experiments were performed at room temperature (25 °C) in atmospheric pressure, unless stated otherwise. All of the electrochemical measurements were performed with the assistance of a potentiostat/galvanostat system (PGSTAT204, Metrohm Autolab). Ag/AgCl, KCl (sat'd) was set as the reference electrode for all of the electrochemical measurements in this work.

2.2. Preparation of BDD electrode

The polycrystalline BDD film was deposited on a Si (100) wafer substrate with a microwave plasma-assisted chemical vapor deposition (MPCVD) system (AX6500, Cornes Technologies Ltd.). The concentration of boron in the BDD electrode was determined by the ratio between the carbon source (methane) and the boron source (trimethylboron) and was set to 0.1%.[27] A glow discharge optical emission spectroscopy (GD-Profiler2, Horiba Ltd.) measurement was performed to further confirm the exact content of boron in BDD. Raman spectrum was recorded using an Acton SP2500 (Princeton Instruments) with a 532 nm laser (Figure S1) to confirm the crystallinity of diamond and exclude the interference caused by sp^2 carbon.[28] Surface morphology images of the BDD film were obtained with a scanning electron microscope (JCM-6000, JEOL) (Figure S1). The interference of the substrate, Si (100), was excluded by corresponding eCO_2RR (Figure S2, Table S1).

2.3. Electrochemical Measurements and Product Analysis

Before each electrolysis, the BDD electrode was cleaned with 2-propanol and DI water by an ultrasonic treatment for 10 min each. Electrochemical measurements were performed in a two-compartment polytetrafluoroethylene (PTFE) flow cell which was with the same condition of our previous work.[24] 0.1% BDD, Pt, and Ag/AgCl (KCl sat'd) were set as the cathode, anode, and reference electrode, respectively, and the two chambers of the cell were separated by Nafion NRE-212 (Sigma-Aldrich). As a pretreatment before CO_2 reduction, several cyclic voltammetry (CV) scans (including 10 cycles from a potential of −3.5 to 3.5 V and 20 cycles from 0 to 3.5 V in 0.1 M H_2SO_4 and 0.1 M $NaClO_4$, respectively, with a scan rate of 0.5 V/s) were performed to ensure reproducibility and cleanliness of the surface of the electrodes. The catholyte and anolyte were 0.5 M KCl and 1 M KOH, respectively (50 mL each). The catholyte was bubbled with N_2 for 30 min to remove oxygen and CO_2 for 60 min, resulting in a CO_2-sauturated solution. During electrolysis, CO_2 bubbling was set at a flow rate of 10 mL min^{-1}.

For the two-electrode electrolysis system, the nafion membrane was replaced by the bipolar membrane (fumasep FBM, FUELCELL Store). Each chamber in the cell was connected with a reference electrode (Ag/AgCl, KCl sat'd) to monitor the working potentials of both cathode and anode. In comparison experiments, the Pt anode was further replaced by Ni (Nilaco), $NiFeO_x$, and dimensional stable electrode (DSE, DE NORA). The $NiFeO_x$ electrode was synthesized through electrodeposition. In brief, a Ni foil was immersed in a mixture solution of 9 mM $NiSO_4$, 9 mM $FeSO_4$, and 25 mM $(NH_4)_2SO_4$ (pH adjusted at 2.5 by H_2SO_4) and was electrolyzed under a constant current of 10 mA/cm^2 for 30 s and repeated for 50 cycles.

At the end of each CO_2 reduction experiment, all of the products were quantified. Formic acid was quantified by high-performance liquid chromatography (HPLC, CDD-10A, Shimadzu Corp.). The gaseous products (CO and H_2) were collected in an aluminum gas bag (GL Sciences) and quantified by gas chromatography (GC-2014, Shimadzu Corp.). Formic acid for HPLC calibration was obtained from FUJIFILM Wako pure Chemical Corporation. Hydrogen and carbon monoxide for GC calibration were obtained from GL Sciences.

2.4. XPS Measurements

The specific elemental information about the surface of BDD electrode was measured with an X-ray photoelectron spectrometer (XPS, JPS-9010 TR, JEOL). The C 1s spectra were deconvoluted with Gaussian functions. Peaks deconvoluted from the C 1s spectra were assigned to the following components: 283.0 eV (sp^2 C−C bond), 284.1 eV (C−H bond), 284.75 eV (sp^3 C−C bond), 285.3 eV (C−O bond), and 286.2 eV (C═O bond). These binding energies were fixed for all of the XPS analyses.

2.5. In Situ Attenuated Total Reflectance Infrared Spectroscopy Measurements

A thin 0.1% BDD film was deposited on a Si attenuated total reflectance infrared (ATR-IR) prism using MPCVD with the same method as mentioned before. The quality of the BDD film was verified by Raman spectrum (Figure S3). A one chamber PTFE cell was used to perform the electrolysis in which BDD, glassy carbon rod, and Ag/AgCl (KCl sat'd) were set as the working electrode, counter electrode, and reference electrode, respectively. Supporting electrolytes as 0.1 M H_2SO_4 and 0.1 M $NaClO_4$ were used for the pretreatment, while 0.5 M KCl for CO_2RR. The ATR-IR spectra were measured through a FT/IR-6600 (JASCO Corp.) with a liquid-nitrogen-cooled mercury-cadmium-telluride detector. All of the spectra were collected at a resolution of 4 cm^{-1} and had 256 scans. The baseline spectrum and pretreated comparison spectrum were measured in N_2-saturated DI water. After the electrolysis, the BDD electrode was washed by DI water for three times, and then the ATR-IR spectrum was measured again in N_2-saturated DI water.

https://doi.org/10.1021/jacsau.2c00081
JACS Au 2022, 2, 1375−1382

2.6. Modification with Aminoferrocene and Characterization

The BDD electrode was activated by incubation with 10 mM 1-(3-(dimethylamino)propyl)-3-ethylcarbodiimide hydrochloride (EDC, Tokyo Chemical Industry Co. Ltd.), 10 mM *N*-hydroxysuccinimide (NHS, Sigma-Aldrich), and 0.1 M 2-morpholinoethanesulfonic acid (MES, DOJINDO) for 1 h in DI water. After rinsed with 0.1 M MES, the BDD electrode was further incubated with 0.01 M aminoferrocene (Fc-NH_2, Sigma-Aldrich) in 0.1 M carbonate buffer solution (pH 9.8) for 1 h. Fc-NH_2 was previously dissolved in the minimum amount of acetonitrile. Before electrochemical measurements, BDD was rinsed with the mixed solvent DI water and acetonitrile 50:50 v/v. Cyclic voltammetry (CV) scan rate was set to 50 mV s^{-1}, and potential range was from −0.2 to 0.6 V. Square wave voltammetry (SWV) measurements were performed with the scan rate of 50 mV s^{-1} in the potential range of 0.1−0.6 V. All measurements were performed in a one chamber PTFE cell with 0.5 M KCl as supporting electrolyte.

3. RESULTS AND DISCUSSION

3.1. Self-Activation Process of BDD

To investigate and verify the self-activation process of BDD, we first performed the eCO_2RR with a BDD cathode in a three-electrode system in a flow cell. As shown in Figure 1A,B, 3 h eCO2RR experiments were carried out at the potential of −2 V.

Galvanostatic CO_2 reductions for 1 h at current densities of −0.1 mA cm^{-2}, −0.5 mA cm^{-2}, −1 mA cm^{-2}, −1.5 mA cm^{-2}, and −2 mA cm^{-2} were adopted as activation processes and performed before the formal eCO_2RR. Without activation, current density and Faradaic efficiency at BDD are −0.17 mA cm^{-2} and 73.81%, respectively. In contrast, by the activation processes, the current density reached −0.22 mA cm^{-2}, −0.3 mA cm^{-2}, −0.59 mA cm^{-2}, −0.23 mA cm^{-2}, and −0.35 mA cm^{-2}, and the Faradaic efficiency for formic acid achieved 81.29%, 88.65%, 91.01%, 87.51%, and 87.32%, respectively. An activation current of −1 mA cm^{-2} resulted in the best conditions, as the current density was improved more than three times and the Faradaic efficiency increased by 17.2% compared to BDD without activation.

To confirm the benefit of activation, electrolysis experiments of eCO_2RR were performed at different potentials from −2.2 V to −1.8 V, where the activation current density was set as −1 mA cm^{-2}. According to Figure 1C, an improvement of the Faradaic efficiency took place in the region of low potentials, also associated with higher current densities and product concentration (Figure S4), indicating that the reaction current of the activated BDD was significantly improved. When the reduction potential was −2.2 V, the Faradaic efficiencies of the activated and nonactivated BDD were at the same level, while at reaction potentials of −2 V, −1.9 V, and −1.8 V, the Faradaic efficiencies of the activated BDD increase of 17.2%, 18.72% and 20.7%, respectively, compared with those by nonactivated BDD.

Previously, we proposed that the generation of $CO_2^{\bullet-}$ intermediate (E^0 = −2.05 V vs Ag/AgCl, KCl (sat'd)) is a reliable pathway for BDD cathode to achieve efficient eCO_2RR.[24,25] Without the activation process, a Faradaic efficiency higher than 80% could be realized only when the applied potential is sufficiently negative to generate the $CO_2^{\bullet-}$. However, the results in Figure 1 proved that with the aid of the activation process, the performance of eCO_2RR was greatly improved for more positive potentials (∼100−150 mV) and a Faradaic efficiency of more than 80% could be obtained even at potentials where the $CO_2^{\bullet-}$ was hardly produced. Besides, it is worth noting that in the eCO_2RR with BDD cathode, the faradic current keeps increasing with time, a tendency observed previously.[29] Therefore, we speculate that during eCO_2RR, BDD will be subjected to a self-activation process that increases the electroactive area available for CO_2 reduction, and reaction intermediates other than $CO_2^{\bullet-}$ might be generated on the surface which will gradually increase along with the reaction time.

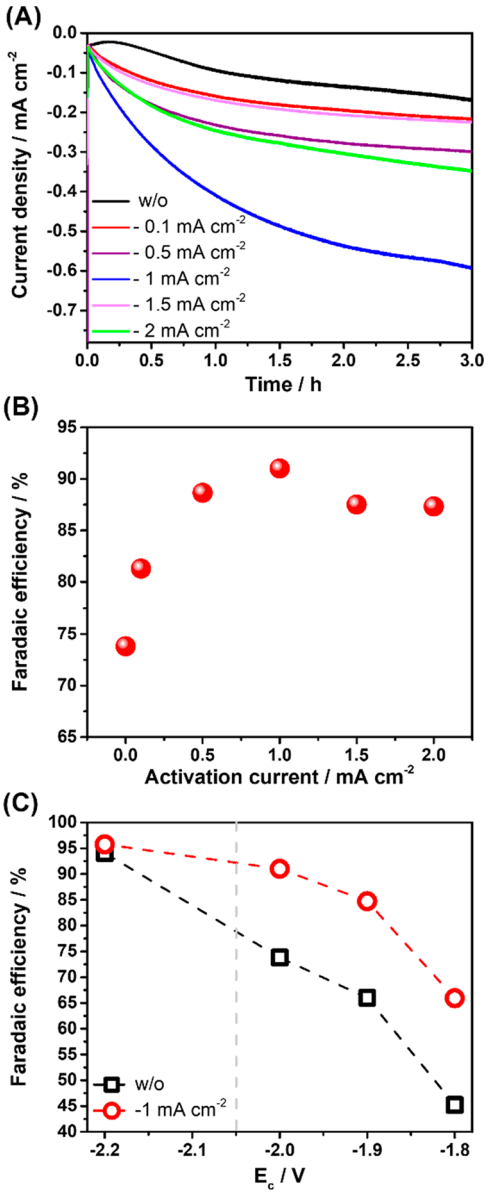

Figure 1. (A) Current densities and (B) Faradaic efficiencies in 3 h eCO_2RR at −2 V showing the difference between the activated and nonactivated BDD electrode. Activation processes were performed with 1 h galvanostatic CO_2 reduction at the current densities of −0.1 mA cm^{-2}, −0.5 mA cm^{-2}, −1 mA cm^{-2}, −1.5 mA cm^{-2}, and −2 mA cm^{-2}, respectively, before the formal eCO_2RR. (C) Compared Faradaic efficiencies of the activated (−1 mA cm^{-2}, red) and nonactivated (w/o, black) BDD electrode at different electrolysis potentials (Ec). Reference electrode: Ag/AgCl, KCl (sat'd). The gray dotted line represents the standard potential of $CO_2/CO_2^{\bullet-}$: E^0 = −2.05 V vs Ag/AgCl, KCl (sat'd).

https://doi.org/10.1021/jacsau.2c00081
JACS Au 2022, 2, 1375−1382

3.2. Mechanistic Investigation

A combination of X-ray photoelectron spectrometer (XPS), in situ attenuated total reflectance infrared (ATR-IR) spectroscopy and electrochemical measurements have been used to investigate the changes of BDD surface state before and after the activation process by eCO_2RR.

The comparison of XPS spectra for C 1s signal was depicted in Figure 2 and fitted to account for five carbon species

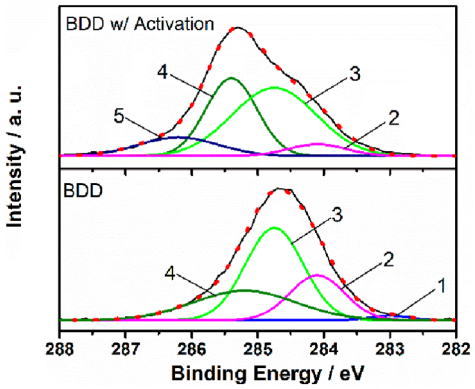

Figure 2. Deconvoluted C 1s spectra for the BDD and BDD with activation electrodes. The components are shown as follows: (1) sp^2 C−C, (2) C−H, (3) sp^3 C−C, (4) C−O, and (5) C═O.

including sp^2 C−C, C−H, sp^3 C−C, C−O, and C═O.[30] The deconvolution of the C 1s signal revealed that with the activation by eCO_2RR, the content of C−H bonds decreased, while the amount of oxygen-containing groups increased, where the increment of C−O bond was 5% and the content of C═O group increased to 12.6%. From this increment of oxygen moieties, we presumed that during eCO_2RR, the CO_2 molecules were first bound on BDD in the form of chemisorption and then reacted into oxygen-containing intermediates. The relative abundance of these components is summarized in Table 1.

Table 1. Relative Abundance of the Components (%) on the Surface of BDD Electrodes

	sp^2 C−C	C−H	sp^3 C−C	C−O	C═O
BDD	1.5	22.3	48.8	27.4	–
BDD w/activation	–	5.8	48.2	33.4	12.6

To confirm the XPS results and verify the existence of such oxygen-containing intermediates, in situ ATR-IR spectroscopy measurements were further carried out (Figure 3). Before eCO_2RR, the background ATR-IR spectrum did not show any feature, even during CO_2 bubbling, meaning that signals of CO_2 chemisorption could not be observed (Figure S5−6). During eCO_2RR, new absorption peaks emerged in the region of 1900 cm^{-1}−1200 cm^{-1} (Figure 3). The strong absorption at 1530−1470 cm^{-1} and 1370−1300 cm^{-1} was assigned to the vibration of unidentate carbonate (−O−CO_2),[31] and showed an increasing trend with time of eCO_2RR. Because the intense absorption peaks at 1650 cm^{-1} and 3400−3200 cm^{-1} showed a similar time-dependent variation (Figure 3 and Figure S7), both have been assigned to water vibration modes.[20] Conversely to water vibrations, the shoulder peak at 1720−1710 cm^{-1} kept increasing during the eCO_2RR. Therefore, we suggested that the shoulder peak at 1720−1710 cm^{-1} and peak

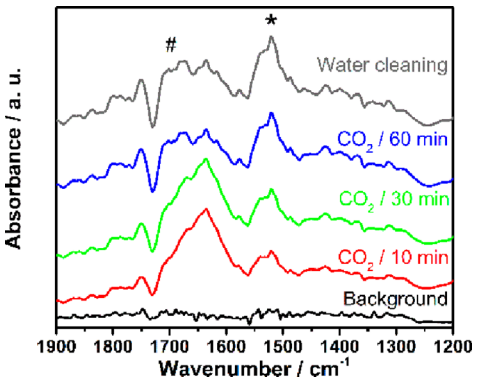

Figure 3. In situ time-dependent ATR-IR spectra during CO_2 reduction at −2 V vs Ag/AgCl, KCl (sat'd). The gray line shows the ATR-IR spectrum after rinsing BDD in ultrapure water. * and # indicate the υ_4 vibration of unidentate carbonate and the stretching vibration of carboxylic C═O group, respectively.

at 1460−1370 cm^{-1} could be assigned to the characteristic absorption of C═O and −OH groups in carboxylic structure (−COOH), respectively;[32] moreover, this signal cannot be mistaken for formic acid in solution (Figure S8). Even after rinsing the BDD in ultrapure water, the characteristic peaks of unidentate carbonate and carboxylic structure on the surface could be observed clearly (Figure 3). In addition, the presence of the carboxylic structure on BDD after eCO_2RR was further verified by reaction with aminoferrocene (Fc-NH_2, Figure S9)[33,34] and detected electrochemically (Figure 4A).

The schematic diagram showing the modification process of Fc-NH_2 was described in Figure S9. With the help of 1-(3-(dimethylamino)propyl)-3-ethylcarbodiimide hydrochloride (EDC) and *N*-hydroxysuccinimide (NHS), the carboxylic structure on the surface of BDD can be activated to react with the amino group of Fc-NH_2, and consequently the redox process of Fc-NH_2 can be monitored by CV. A clear redox signal, corresponding to ferrocene, was observed for BDD electrode after eCO_2RR, but not for the comparison BDD (Figure 4A), thus confirming that carboxylic functionalities were available on the surface of BDD only after eCO_2RR. Considering that aldehyde groups can react with Fc-NH_2 as well, and without activation by EDC/NHS, we performed the Fc-NH_2 functionalization without EDC/NHS. Because the CV did not show any redox peak, we could exclude the presence of aldehydes on BDD surface after eCO_2RR (Figure 4A). Therefore, the formation of carboxylic functionalities could be demonstrated through ATR-IR spectra and redox signals from the functionalization with Fc-NH_2. Furthermore, to evaluate the time dependence on the formation of carboxylic groups, we measured the ferrocene redox signal at increasing time of eCO_2RR (Figure 4B). The current increment for the redox peak of ferrocene demonstrates that the amount of carboxylic functionality intermediates generated on the surface of BDD electrode increased gradually with the time of eCO_2RR.

On the basis of the measurements described previously, we demonstrated that during eCO_2RR, unidentate carbonate and carboxylic structure were generated on the surface of BDD. The amount of both intermediates increased with the time of electrolysis, and these two groups could remain on the surface of BDD even after the CO_2 reduction. Therefore, we concluded that CO_2 molecules would be bound on the surface of BDD in the form of unidentate carbonate first, then

https://doi.org/10.1021/jacsau.2c00081
JACS Au 2022, 2, 1375−1382

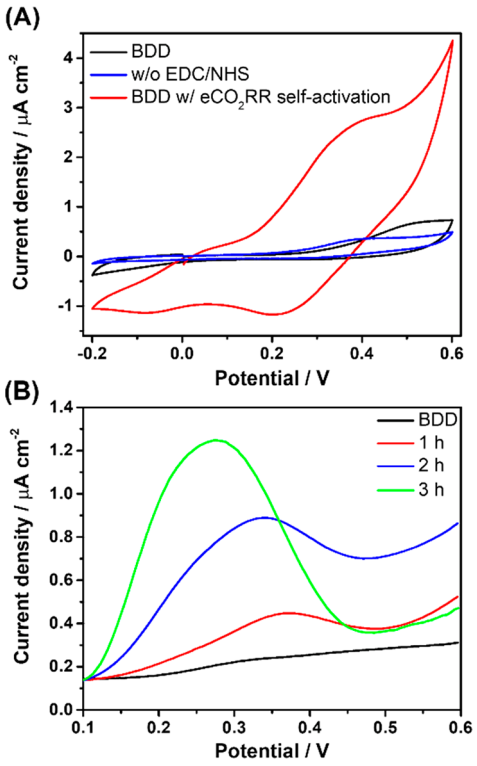

Figure 4. (A) CVs of BDD electrodes after the modification with Fc-NH_2: Comparison sample without CO_2 reduction (black), CO_2 reduction-activated BDD without the addition of EDC/NHS before the Fc-NH_2 functionalization (blue), and CO_2 reduction-activated BDD coupled with the addition of EDC/NHS before the Fc-NH_2 functionalization (red); BDD activation by galvanostatic eCO_2RR at −1 mA cm^{-2}. (B) SWVs showing the variation of the Fc-NH_2 signals along with the time of eCO_2RR. Scan rate: 50 mV s^{-1}, supporting electrolyte: 0.5 M KCl, reference electrode: Ag/AgCl, KCl (sat'd).

underwent a proton-coupled electron transfer reaction[35] at negative potentials to generate carboxylic groups, and finally released from the surface of BDD as formate. During electrolysis, the increase of unidentate carbonate and carboxylic intermediates on the surface of BDD brings the direct consequence of enhancing the Faradaic efficiency of CO_2 reduction because activation will not only improve the reaction current but also enhance the competitiveness of eCO_2RR for protons, which is an essential reactant for both hydrogen evolution and eCO_2RR. The supposed schematic diagram of this pathway is shown in Figure 5 and Figure S10.

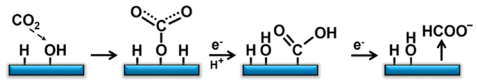

Figure 5. Schematic diagram showing the alternative mechanism of electrochemical CO_2 reduction on BDD at low overpotentials.

In support for the reaction mechanism beyond the experimental evidence, we performed first-principles calculations based on density functional theory. The BLYP functional[36,37] was used to calculate the electronic structures of the surface of interest. The effects of electrolyte solution and electrode potential on the electronic structures were taken into account by using the reference interaction site model[38] and the effective screening medium method,[39] respectively. The surface state with unidentate carbonate was calculated as a stationary point where the negative charge of −0.75 *e* resides on the surface under the experimental electrode potential condition of ca. −2.0 V vs Ag/AgCl (Figure S11A). This starting point has been set at 0 kcal/mol. Concerning the other intermediate, the carboxylic surface state was calculated to be nearly electrically neutral with a neighboring hydroxyl group (Figure S11C). This carboxylic intermediate was found to be more stable by ca. 31 kcal/mol in grand potential than the unidentate carbonate surface state. This result indicates that the reaction proceeds through the unidentate carbonate intermediate followed by the carboxylic structure. The final hydroxyl terminated surface was estimated to be more stable by ca. 85 kcal/mol in grand potential than the carboxylic surface state, which was due to the release of the energy storage compound, that is, formic acid (Figure S11D). Noteworthy, all these defined reaction steps, as reported in Figure 5, proceed exothermically. In conclusion, the calculation results are consistent with the experimental observations and in agreement with the reaction pathway that has been proposed where unidentate carbonate and carboxylic groups are available on the BDD surface. Further insights are available in the Supporting Information (Figure S12 and Table S2).

3.3. Long-Term Self-Activation

To evaluate the time dependence of the self-activation process on BDD and the overall effect on Faradaic and energy efficiency, the eCO_2RR was tested in an electrolysis system. The electrochemical cell comprised two compartments, equipped with a flow electrolyte setup, where BDD was set as the cathode. The electrochemical flow cell was first optimized by testing the performance for different membranes, which separate the anode and cathode chambers (i.e., Nafion and bipolar membrane), and for electrolyte flow rate. As a result, the bipolar membrane was selected to ensure that both sides would not be contaminated by cation crossover, in particular by metal ions from the anode electrode[40,41] (Figures S13−S16), while 400 mL/min was selected as the optimal flow rate of electrolyte (Figure S17 and Tables S3 and S4).

Furthermore, we investigated the performance of four selected anodes such as Pt, Ni, $NiFeO_x$ and dimensional stable electrode (DSE, Ti/IrO_x,Ta_2O_5) to ensure an efficient oxygen evolution reaction (OER).[42] This aspect is crucial because the anode material, completing the electrochemical cell, will affect both the potential distribution between anode and cathode and the current density achievable. The CVs and XPS spectra of anode electrodes are shown in Figures S18 and S19, respectively. We performed the eCO_2RR with the BDD-cathode electrolyzer at different total voltages to find the most suitable potential that maximizes Faradaic efficiency and electrical-to-chemical energy (ECE) conversion efficiency. During this investigation, we observed that both efficiencies are positively correlated with improved OER according to the anode materials. In particular, at 2.7 V the ECE conversion efficiency reached 48%, while the Faradaic efficiency is stable between 85% and 95% (Figure S20 and Tables S5 and S6). The improvement of the ECE conversion efficiency was mainly attributed to the low-energy consumption attained by using efficient OER anodes (Figures S21 and S22 and Tables S7 and S8). The repeatability of the activation process was further verified in two electrode eCO_2RR (Figures S23 and S24).

The time dependence of the self-activation process on BDD was evaluated over 7 h of eCO_2RRs at the best ECE conversion efficiency potential of 2.7 V (Figure S20) by

https://doi.org/10.1021/jacsau.2c00081
JACS Au 2022, 2, 1375−1382

monitoring the current, Faradaic efficiency, and ECE conversion efficiency (Figure 6).

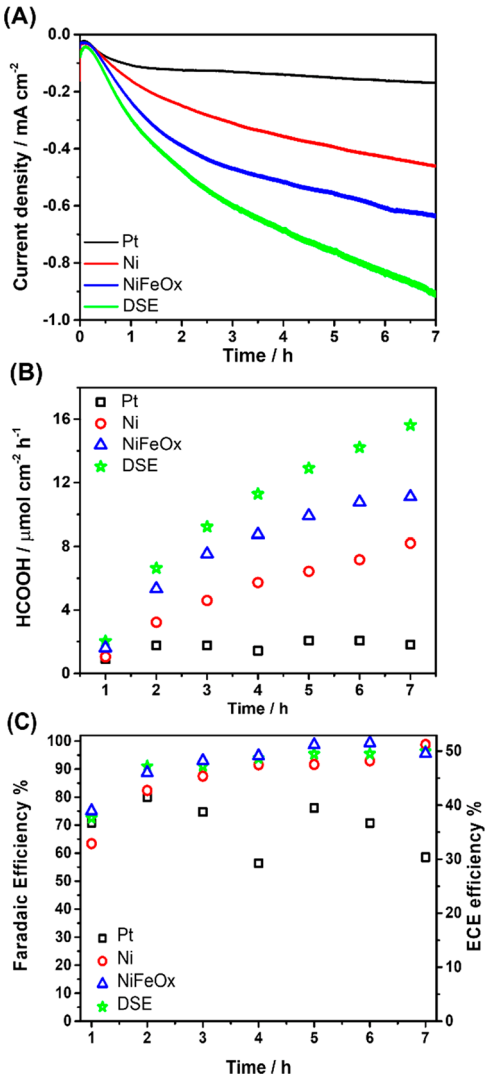

Figure 6. (A) Current densities, (B) production rate, and (C) Faradaic efficiencies/ECE conversion efficiencies of the BDD-based CO_2 electrolyzers which were coupled with different anodes including Pt, Ni, $NiFeO_x$, and DSE. CO_2 reduction electrolysis experiments were performed at the applied voltage of 2.7 V.

Current and formic acid production rate increased continuously with the reaction time, suggesting an ongoing activation of the surface (Figure 6A,B) in agreement with previous results, therefore confirming our hypothesis of BDD "self-activation" during eCO_2RR. The Faradaic efficiency of formic acid could reach more than 90% with an average ECE conversion efficiency of 50.2% after 7 h of continuous eCO_2RR, viz. self-activation (Figure 6C). The effect of different OER anodes is clearly evident in the current values (Figure 6A), as lower overpotentials for OER lead to higher currents and then enhanced self-activation that turns into higher production rates (Figure 6B and Figure S25) with the series DSE(IrO_x) > $NiFeO_x$ > Ni > Pt.

Additionally, we would like to draw attention to the reaction pathways on activated and nonactivated BDD which is the same; this is also the reason to choose the term "self-activation". As shown in Figure 6, in the BDD-based long-term eCO_2RR, both the reaction current density and the Faradaic efficiency for the production of formic acid were continuously improved. This is the essential performance of self-activation, and it indicates that during eCO_2RR, the activity of BDD for CO_2 reduction will keep increasing, which means an improvement of the electroactive surface area. However, due to the low initial reaction current, the process of self-activation is very slow; therefore, it benefits by additional galvanostatic CO_2 reduction performed before the formal eCO_2RR to accelerate the activation process, as demonstrated clearly in Figure 1. A difference in reaction mechanism can be found when the potential is negative enough to generate the $CO_2^{\bullet-}$ which, in that case, provided the same Faradaic efficiency (Figure 1).

Finally, we compared the ECE conversion efficiency of the present work with other representative electrocatalysts,[29,40,41,43−49] to show that BDD can reach remarkable performances (Figure 7). Although the efficiency of BDD does

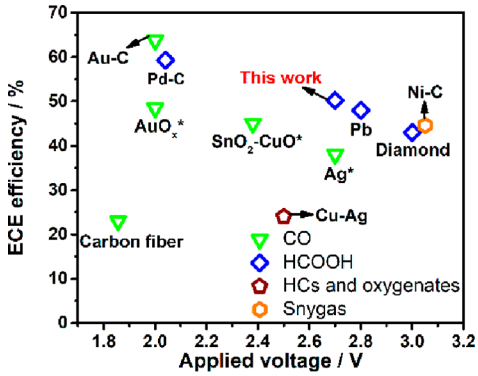

Figure 7. Summarized ECE conversion efficiencies of the reported representative CO_2 electrolyzers. The energy efficiencies with * were calculated by ourselves.

not reach the level of noble metal electrocatalysts (e.g., Au or Pd), the advantages of BDD are in terms of raw material cost, chemical resistance, and physical stability in long-term applications where the carbon nanostructure coupled with noble metal electrocatalysts face structural changes and activity loss.[50,51] We are aware that at present, the electrolysis current density of BDD cannot meet the standard of the industrial application, therefore improving the current density of BDD, for example, by gas diffusion electrode system, will be our research direction for the future work.

CONCLUSION

Here we investigated the mechanism of CO_2 reduction on BDD highlighting a new and until now uncovered mechanism which leads to "self-activation" of the BDD surface during the eCO_2RR. Characterization of the BDD surface by spectroscopic techniques such as XPS and ATR-IR combined with electrochemical analysis with aminoferrocene demonstrated that unidentate carbonate and carboxylic intermediates were generated on the surface of BDD and kept increasing during eCO_2RR. Based on the presence of these intermediates, a new pathway for electrochemical CO_2 reduction was proposed, which was independent of the generation of $CO_2^{\bullet-}$. The CO_2 molecules from the solution first adsorb on the BDD surface as unidentate carbonate and under the application of a suitable negative potential, and the unidentate carbonate is converted

https://doi.org/10.1021/jacsau.2c00081
JACS Au 2022, 2, 1375−1382

to a carboxylic intermediate and finally to formate. During eCO_2RR an increasing amount of carboxylic intermediates are generated on the BDD surface, meaning an improvement of the electroactive surface area in a process we refer as "self-activation" that improves both reaction current and Faradaic efficiency of eCO_2RR. The technological application performance of the self-activation effect was further estimated by 7 h eCO_2RR in a flow electrolyzer. Benefiting from the self-activation effect, the BDD electrode reaches an ECE conversion efficiency of 50.2% for the single product of formic acid. This work provides new insights on the mechanism of electrochemical CO_2 reduction at BDD electrodes and demonstrates its potential application as working electrode for eCO_2RR.

■ ASSOCIATED CONTENT

Supporting Information

The Supporting Information is available free of charge at https://pubs.acs.org/doi/10.1021/jacsau.2c00081.

Details for the "self-activation" process for BDD electrode, the computational methods and calculation results, nafion and bipolar membrane: optimization experiments, electrolyte flow rate; optimization experiments, anode electrodes characterizations, Faradaic efficiency and ECE conversion efficiency, calculation of the energy distribution in the two-electrodes cell, Faradaic efficiency, ECE conversion efficiency, and energy distribution in the two-electrodes cell; results and Raman spectra of BDD electrodes (PDF)

■ AUTHOR INFORMATION

Corresponding Author

Yasuaki Einaga − *Department of Chemistry, Keio University, Yokohama 223-8522, Japan;* orcid.org/0000-0001-7057-4358; Email: einaga@chem.keio.ac.jp

Authors

Jinglun Du − *Department of Chemistry, Keio University, Yokohama 223-8522, Japan*

Andrea Fiorani − *Department of Chemistry, Keio University, Yokohama 223-8522, Japan*

Taichi Inagaki − *Department of Chemistry, Keio University, Yokohama 223-8522, Japan*

Atsushi Otake − *Department of Chemistry, Keio University, Yokohama 223-8522, Japan*

Michio Murata − *Department of Chemistry, Keio University, Yokohama 223-8522, Japan*

Miho Hatanaka − *Department of Chemistry, Keio University, Yokohama 223-8522, Japan*

Complete contact information is available at: https://pubs.acs.org/10.1021/jacsau.2c00081

Notes

The authors declare no competing financial interest.

■ ACKNOWLEDGMENTS

The authors thank Sumitomo Heavy Industries, Ltd. for useful discussions. A.F. acknowledges the Japan Society for the Promotion of Science (fellowship ID no. P19333) and Grant-in-Aid for JSPS Fellows (19F19333). Also, this work was partially supported by Grant-in-Aid for Scientific Research A 19H00832 and New Energy and Industrial Technology Development Organization (NEDO) P16002 (to Y.E.).

■ ABBREVIATIONS

BDD, boron-doped diamond; eCO_2RR, electrochemical carbon dioxide reduction reaction; ECE, electrical-to-chemical energy

■ REFERENCES

(1) Aresta, M.; Dibenedetto, A.; Angelini, A. Catalysis for the Valorization of Exhaust Carbon: From CO2 to Chemicals, Materials, and Fuels. Technological Use of CO2. *Chem. Rev.* **2014**, *114* (3), 1709−1742.

(2) Goeppert, A.; Czaun, M.; Jones, J. P.; Surya Prakash, G. K.; Olah, G. A. Recycling of Carbon Dioxide to Methanol and Derived Products-Closing the Loop. *Chem. Soc. Rev.* **2014**, *43* (23), 7995−8048.

(3) Matthessen, R.; Fransaer, J.; Binnemans, K.; De Vos, D. E. Electrocarboxylation: Towards Sustainable and Efficient Synthesis of Valuable Carboxylic Acids. *Beilstein J. Org. Chem.* **2014**, *10*, 2484−2500.

(4) Fiorani, G.; Guo, W.; Kleij, A. W. Sustainable Conversion of Carbon Dioxide: The Advent of Organocatalysis. *Green Chem.* **2015**, *17* (3), 1375−1389.

(5) Nielsen, D. U.; Hu, X. M.; Daasbjerg, K.; Skrydstrup, T. Chemically and Electrochemically Catalysed Conversion of CO2 to CO with Follow-up Utilization to Value-Added Chemicals. *Nat. Catal.* **2018**, *1* (4), 244−254.

(6) Kondratenko, E. V.; Mul, G.; Baltrusaitis, J.; Larrazábal, G. O.; Pérez-Ramírez, J. Status and perspectives of CO2 conversion into fuels and chemicals by catalytic, photocatalytic and electrocatalytic processes. *Energy Environ. Sci.* **2013**, *6* (11), 3112−3135.

(7) Verma, S.; Kim, B.; Jhong, H. R. M.; Ma, S.; Kenis, P. J. A. A gross-margin model for defining technoeconomic benchmarks in the electroreduction of CO_2. *ChemSusChem* **2016**, *9* (15), 1972−1979.

(8) Whipple, D. T.; Kenis, P. J. A. Prospects of CO_2 utilization via direct heterogeneous electrochemical reduction. *J. Phys. Chem. Lett.* **2010**, *1* (24), 3451−3458.

(9) Singh, A. K.; Singh, S.; Kumar, A. Hydrogen energy future with formic acid: A renewable chemical hydrogen storage system. *Catal. Sci. Technol.* **2016**, *6* (1), 12−40.

(10) Yu, X.; Pickup, P. G. Recent advances in direct formic acid fuel cells (DFAFC). *J. Power Sources* **2008**, *182* (1), 124−132.

(11) Bushuyev, O. S.; De Luna, P.; Dinh, C. T.; Tao, L.; Saur, G.; van de Lagemaat, J.; Kelley, S. O.; Sargent, E. H. What Should We Make with CO_2 and How Can We Make It? *Joule* **2018**, *2* (5), 825−832.

(12) Kortlever, R.; Shen, J.; Schouten, K. J. P.; Calle-Vallejo, F.; Koper, M. T. M. Catalysts and Reaction Pathways for the Electrochemical Reduction of Carbon Dioxide. *J. Phys. Chem. Lett.* **2015**, *6* (20), 4073−4082.

(13) White, J. L.; Baruch, M. F.; Pander, J. E.; Hu, Y.; Fortmeyer, I. C.; Park, J. E.; Zhang, T.; Liao, K.; Gu, J.; Yan, Y.; Shaw, T. W.; Abelev, E.; Bocarsly, A. B. Light-Driven Heterogeneous Reduction of Carbon Dioxide: Photocatalysts and Photoelectrodes. *Chem. Rev.* **2015**, *115* (23), 12888−12935.

(14) Koppenol, W. H.; Rush, J. D. Reduction potential of the carbon dioxide/carbon dioxide radical anion: a comparison with other C1 radicals. *J. Phys. Chem.* **1987**, *91* (16), 4429−4430.

(15) Lamy, E.; Nadjo, L.; Saveant, J. M. Standard potential and kinetic parameters of the electrochemical reduction of carbon dioxide in dimethylformamide. *J. Electroanal. Chem.* **1977**, *78* (2), 403−407.

(16) Lin, B.; Golshan-Shirazi, S.; Guiochon, G. Effect of mass transfer coefficient on the elution profile in nonlinear chromatography. *J. Phys. Chem.* **1989**, *93* (8), 3363.

(17) Schwarz, H. A.; Dodson, R. W. Reduction potentials of CO_2- and the alcohol radicals. *J. Phys. Chem.* **1989**, *93* (1), 409−414.

(18) Chen, Y.; Li, C. W.; Kanan, M. W. Aqueous CO_2 reduction at very low overpotential on oxide-derived au nanoparticles. *J. Am. Chem. Soc.* **2012**, *134* (49), 19969−19972.
(19) Chen, Y.; Kanan, M. W. Tin oxide dependence of the CO_2 reduction efficiency on tin electrodes and enhanced activity for tin/tin oxide thin-film catalysts. *J. Am. Chem. Soc.* **2012**, *134* (4), 1986−1989.
(20) Baruch, M. F.; Pander, J. E.; White, J. L.; Bocarsly, A. B. Mechanistic Insights into the Reduction of CO_2 on Tin Electrodes using in Situ ATR-IR Spectroscopy. *ACS Catal.* **2015**, *5* (5), 3148−3156.
(21) Valenti, G.; Melchionna, M.; Montini, T.; Boni, A.; Nasi, L.; Fonda, E.; Criado, A.; Zitolo, A.; Voci, S.; Bertoni, G.; Bonchio, M.; Fornasiero, P.; Paolucci, F.; Prato, M. Water-Mediated Electro-Hydrogenation of CO_2 at Near-Equilibrium Potential by Carbon Nanotubes/Cerium Dioxide Nanohybrids. *ACS Appl. Energy Mater.* **2020**, *3* (9), 8509−8518.
(22) Ikemiya, N.; Natsui, K.; Nakata, K.; Einaga, Y. Long-Term Continuous Conversion of CO_2 to Formic Acid Using Boron-Doped Diamond Electrodes. *ACS Sustain. Chem. Eng.* **2018**, *6* (7), 8108−8112.
(23) Kashiwada, T.; Watanabe, T.; Ootani, Y.; Tateyama, Y.; Einaga, Y. A Study on Electrolytic Corrosion of Boron-Doped Diamond Electrodes when Decomposing Organic Compounds. *ACS Appl. Mater. Interfaces* **2016**, *8* (42), 28299−28305.
(24) Natsui, K.; Iwakawa, H.; Ikemiya, N.; Nakata, K.; Einaga, Y. Stable and Highly Efficient Electrochemical Production of Formic Acid from Carbon Dioxide Using Diamond Electrodes. *Angew. Chemie - Int. Ed.* **2018**, *57* (10), 2639−2643.
(25) Tomisaki, M.; Kasahara, S.; Natsui, K.; Ikemiya, N.; Einaga, Y. Switchable Product Selectivity in the Electrochemical Reduction of Carbon Dioxide Using Boron-Doped Diamond Electrodes. *J. Am. Chem. Soc.* **2019**, *141* (18), 7414−7420.
(26) Einaga, Y. Diamond electrodes for electrochemical analysis. *J. Appl. Electrochem.* **2010**, *40* (10), 1807−1816.
(27) Xu, J.; Natsui, K.; Naoi, S.; Nakata, K.; Einaga, Y. Effect of Doping Level on the Electrochemical Reduction of CO_2 on Boron-Doped Diamond Electrodes. *Diam. Relat. Mater.* **2018**, *86*, 167−172.
(28) Xu, J.; Einaga, Y. Effect of Sp2 Species in a Boron-Doped Diamond Electrode on the Electrochemical Reduction of CO_2. *Electrochem. commun.* **2020**, *115*, 106731.
(29) Du, J.; Fiorani, A.; Einaga, Y. An efficient, formic acid selective CO_2 electrolyzer with a boron-doped diamond cathode. *Sustain. Energy Fuels* **2021**, *5* (10), 2590−2594.
(30) Kasahara, S.; Natsui, K.; Watanabe, T.; Yokota, Y.; Kim, Y.; Iizuka, S.; Tateyama, Y.; Einaga, Y. Surface Hydrogenation of Boron-Doped Diamond Electrodes by Cathodic Reduction. *Anal. Chem.* **2017**, *89* (21), 11341−11347.
(31) Thornton, E. W.; Harrison, P. G. Tin Oxide surfaces part 1. *J. Chem. Soc., Faraday Trans. 1* **1975**, *71*, 461−472.
(32) Cagnon, B.; Py, X.; Guillot, A.; Joly, J. P.; Berjoan, R. Pore structure modification of pitch-based activated carbon by NaOCl and air oxidation/pyrolysis cycles. *Microporous Mesoporous Mater.* **2005**, *80* (1−3), 183−193.
(33) Dolci, L. S.; Quiroga, S. D.; Gherardi, M.; Laurita, R.; Liguori, A.; Sanibondi, P.; Fiorani, A.; Calzà, L.; Colombo, V.; Focarete, M. L. Carboxyl surface functionalization of poly(L -lactic acid) electrospun nanofibers through atmospheric non-thermal plasma affects fibroblast morphology. *Plasma Process. Polym.* **2014**, *11* (3), 203−213.
(34) Věžník, J.; Konhefr, M.; Trnková, L.; Skládal, P.; Lacina, K. Elusive pKa' of aminoferrocene determined with voltammetric methods in buffered and unbuffered systems and practical aspects of such experiments. *Electrochim. Acta* **2019**, *318*, 534−541.
(35) Costentin, C.; Robert, M.; Savéant. Catalysis of the electrochemical reduction of carbon dioxide. J. M. *Chem. Soc. Rev.* **2013**, *42* (6), 2423−2436.
(36) Becke, A. D. Density-Functional Exchange-Energy Approximation with Correct Assymptonic Behaviour. *Phys. Rev. A* **1988**, *38*, 3098−3100.
(37) Lee, C.; Yang, W.; Parr, R. G. Development of the Colle-Salvetti Correlation-Energy Formula into a Functional of the Electron Density. *Phys. Rev. B* **1988**, *37*, 785−789.
(38) Nishihara, S.; Otani, M. Hybrid solvation models for bulk, interface, and membrane: Reference interaction site methods coupled with density functional theory. *Phys. Rev. B* **2017**, *96* (11), 2−3.
(39) Otani, M.; Sugino, O. First-principles calculations of charged surfaces and interfaces: A plane-wave nonrepeated slab approach. *Phys. Rev. B - Condens. Matter Mater. Phys.* **2006**, *73* (11), 1−11.
(40) Zhou, X.; Liu, R.; Sun, K.; Chen, Y.; Verlage, E.; Francis, S. A.; Lewis, N. S.; Xiang, C. Solar-Driven Reduction of 1 atm of CO_2 to Formate at 10% Energy-Conversion Efficiency by Use of a TiO_2-Protected III-V Tandem Photoanode in Conjunction with a Bipolar Membrane and a Pd/C Cathode. *ACS Energy Lett.* **2016**, *1*, 764−770.
(41) Vermaas, D. A.; Smith, W. A. Synergistic Electrochemical CO_2 Reduction and Water Oxidation with a Bipolar Membrane. *ACS Energy Lett.* **2016**, *1* (6), 1143−1148.
(42) McCrory, C. C. L.; Jung, S.; Peters, J. C.; Jaramillo, T. F. Benchmarking heterogeneous electrocatalysts for the oxygen evolution reaction. *J. Am. Chem. Soc.* **2013**, *135* (45), 16977−16987.
(43) Yamamoto, T.; et al. Electrochemical Reduction of CO_2 in the Micropores of Activated Carbon Fibers. *J. Electrochem. Soc.* **2000**, *147*, 3393−3400.
(44) Verma, S.; Hamasaki, Y.; Kim, C.; Huang, W.; Lu, S.; Jhong, H. R. M.; Gewirth, A. A.; Fujigaya, T.; Nakashima, N.; Kenis, P. J. A. Insights into the Low Overpotential Electroreduction of CO_2 to CO on a Supported Gold Catalyst in an Alkaline Flow Electrolyzer. *ACS Energy Lett.* **2018**, *3* (1), 193−198.
(45) Lu, X.; Leung, D. Y. C.; Wang, H.; Xuan, J. A high performance dual electrolyte microfluidic reactor for the utilization of CO_2. *Appl. Energy* **2017**, *194*, 549−559.
(46) Gurudayal; Bullock, J.; Srankó, D. F.; Towle, C. M.; Lum, Y.; Hettick, M.; Scott, M. C.; Javey, A.; Ager, J. Efficient solar-driven electrochemical CO_2 reduction to hydrocarbons and oxygenates. *Energy Environ. Sci.* **2017**, *10* (10), 2222−2230.
(47) Yamamoto, T.; Tryk, D. A.; Fujishimal, A.; Ohata, H. Production of syngas plus oxygen from CO_2 in a gas-diffusion electrode-based electrolytic cell. *Electrochim. Acta* **2002**, *47* (20), 3327−3334.
(48) Schreier, M.; Curvat, L.; Giordano, F.; Steier, L.; Abate, A.; Zakeeruddin, S. M.; Luo, J.; Mayer, M. T.; Grätzel, M. Efficient photosynthesis of carbon monoxide from CO_2 using perovskite photovoltaics. *Nat. Commun.* **2015**, *6*, 7326.
(49) Gurudayal, G.; Bullock, J.; Sranko, D. F.; Towle, C. M.; Lum, Y.; Hettick, M.; Scott, M. C.; Javey, A.; Ager, J. Efficient solar driven electrochemical CO_2 reduction to hydrocarbons and oxygenates. *Energy Environ. Sci.* **2017**, *10* (10), 2222−2230.
(50) Hegge, F.; Sharman, J.; Moroni, R.; Thiele, S.; Zengerle, R.; Breitwieser, M.; Vierrath, S. Impact of Carbon Support Corrosion on Performance Losses in Polymer Electrolyte Membrane Fuel Cells. *J. Electrochem. Soc.* **2019**, *166* (13), F956−F962.
(51) Li, F.; Medvedeva, X. V.; Medvedev, J. J.; Khairullina, E.; Engelhardt, H.; Chandrasekar, S.; Guo, Y.; Jin, J.; Lee, A.; Thérien-Aubin, H.; Ahmed, A.; Pang, Y.; Klinkova, A. Interplay of electrochemical and electrical effects induces structural transformations in electrocatalysts. *Nat. Catal.* **2021**, *4* (6), 479−487.

https://doi.org/10.1021/jacsau.2c00081
JACS Au 2022, 2, 1375−1382